Terahertz Reading of Ferroelectric Domain Wall Dielectric Switching

Man Zhang,[1] Zhe Chen,[2,8] Yajun Yue,[3] Tao Chen,[3] Zhongna Yan,[3,7] Qinghui Jiang,[4] Bin Yang[2,], Mirva Eriksson,[5] Jianhua Tang,[6] Dou Zhang,[7,*] Zhijian Shen,[5] Isaac Abrahams[3] and Haixue Yan[1,*]*

[1] School of Engineering and Materials Science, Queen Mary University of London

Mile End Road, London, E1 4NS, United Kingdom

[2] Faculty of Science and Engineering, University of Chester

Thornton Science Park, Chester, CH2 4NU, United Kingdom

[3] School of Biological and Chemical Sciences, Queen Mary University of London

Mile End Road, London, E1 4NS, United Kingdom

[4] School of Materials Science and Engineering, Huazhong University of Science and Technology, Luoyu Road, Wuhan, 430074, China

[5] Department of Materials and Environmental Chemistry, Stockholm University

S-10691, Sweden

[6] Cancer Research UK Manchester Institute, The University of Manchester

Oxford Road, Manchester, SK10 4TG, United Kingdom

[7] State Key Laboratory of Powder Metallurgy, Central South University

South Lushan Road, Changsha, 410083, China

[8] College of electronic information engineering, South-central University for Nationalities

Minyuan Road, Wuhan, 430074, China

KEYWORDS: domain wall, ferroelectric, dielectric, lead free, Terahertz probe

ABSTRACT

Ferroelectric domain walls (DWs) are important nano scale interfaces between two domains. It is widely accepted that ferroelectric domain walls work idly at terahertz (THz) frequencies, consequently discouraging efforts to engineer the domain walls to create new applications that utilise THz radiation. However, the present work clearly demonstrates the activity of domain walls at THz frequencies in a lead free Aurivillius phase ferroelectric ceramic, $Ca_{0.99}Rb_{0.005}Ce_{0.005}Bi_2Nb_2O_9$, examined using THz time domain spectroscopy (THz-TDS). The dynamics of domain walls are different at kHz and THz frequencies. At low frequencies, domain walls work as a group to increase dielectric permittivity. At THz frequencies, the defective nature of domain walls serves to lower the overall dielectric permittivity. This is evidenced by higher dielectric permittivity in the THz band after poling, reflecting decreased domain wall density. An elastic vibrational model has also been used to verify that a single frustrated dipole in a domain wall represents a weaker contribution to the permittivity than its counterpart within a domain. The work represents a fundamental breakthrough in understanding dielectric contributions of domain walls at THz frequencies. It also demonstrates that THz probing can be used to read domain wall dielectric switching.

1. INTRODUCTION

Ferroelectric materials are commonly used in dielectric capacitors,[1] piezoelectric sensors, actuators[2,3] and ferroelectric memories for data storage.[4–6] The properties of ferroelectrics are often dominated by the density and activity of their domain walls.[7–11] Domain wall engineering can be used to optimise dielectric,[12–15] piezoelectric[16,17] and ferroelectric properties[18,19] and hence develop new applications. At present, lead zirconate-titanate (PZT) ceramics are the most widely used commercial ferroelectrics.[20] Experiments have shown that more than 60% of dielectric and piezoelectric responses in PZT ceramics are caused from the contribution of domain walls at room temperature.[21,22] Landau-Ginzburg-Devonshire theory also reveals that effective piezoelectric response across 90° domain walls is much higher than that in the single-domain region in tetragonal ferroelectrics.[23] Although the contribution from domain walls has been extensively investigated in different ferroelectrics at lower frequencies (kHz), their contribution at terahertz (THz) frequencies has received less attention as it is assumed that the domain walls are only active below 10^{10} Hz.[24] The domain wall dynamics at the THz frequencies are still an open question and a fundamental understanding is a key step towards new applications of ferroelectrics at these higher electromagnetic frequencies.

Aurivillius phase ferroelectrics are good candidate materials for non-volatile memory and high-temperature piezoelectric sensors due to their fatigue-resistance[5] and high Curie points (T_c),[25] respectively. $CaBi_2Nb_2O_9$ (CBNO) is a ferroelectric with the highest T_c amongst the Aurivillius phase compounds.[26] Pure CBNO exhibits orthorhombic symmetry in space group $A2_1am$ with spontaneous polarization (P_s) parallel to the *a*-

axis.[27] Due to its layered structure, ferroelectric switching is restricted to directions perpendicular to the layer axis (*c*-axis). However, the thermal stability of dielectric permittivity of pure CBNO is low,[28] which limits its commercial use. In order to improve the thermal stability of dielectric permittivity, a doping approach has been used here in the system $Ca_{0.99}Rb_{0.005}Ce_{0.005}Bi_2Nb_2O_9$ (CBNRC). The dynamics of CBNRC's domain walls at the THz band are investigated by THz-time domain spectroscopy (THz-TDS) and low frequency impedance measurements are implemented for complementary analysis. Moreover, an elastic vibrational model has been theoretically constructed to interpret the differential dynamics of a single electric dipole under an alternating electric field in domains and domain walls. The work not only shows that the contribution of ferroelectric domain walls to dielectric permittivity at THz frequencies is non-negligible, but also demonstrates the possibility of new devices based on non-destructive read-out dielectric switching memory, readable by THz probe.

2. EXPERMIENTAL AND SIMULATION METHOD

$Ca_{0.99}Rb_{0.05}Ce_{0.05}Bi_2Nb_2O_9$ ceramic was prepared by conventional solid-state reaction. Stoichiometric quantities of $CaCO_3$ (99.9% purity), Bi_2O_3 (99.9%), Nb_2O_5 (99.5%), Rb_2CO_3 (99.8%) and CeO_2 (99.9%) were ball milled together for 4 h, using ethanol as the milling medium. The slurry was dried overnight at 80 °C to remove ethanol. The dried mixture was successively calcined at 800 °C for 2 h and 950 °C for 2 h and subsequently re-milled for 4 h in ethanol and dried. Polyvinyl alcohol (PVA, 5%) was then added to the calcined powder as a binder and the powder was pressed into 13 mm pellets at 150 MPa. The pellets were heated at 650 °C for 2 h to burn out the PVA and then heated up to

1150 °C and held at this temperature for 2 h to sinter the samples. All heating was carried out in air.

The crystal structure of the ceramic was examined by X-ray diffraction (XRD) in flat-plate Bragg-Brentano mode with a PANAlytical X'Pert Pro diffractometer, fitted with an X'Celerator detector using Ni-filtered Cu Kα radiation (λ = 1.5418 Å). Data were collected in the 2θ range 5 to 120 ° in steps of 0.0167 °, with an equivalent count time of 200 s per step. Structure refinement was carried out with the GSAS suite of programmes. The microstructure of the sample was observed using scanning electron microscopy (FEI Inspect-F) equipped with energy dispersive X-ray spectroscopy (EDX). For electrical property measurements, samples were polished using SiC paper. Pt (for T_c measurements) or Ag electrodes were painted on both surfaces of the polished samples and fired at 950 °C for 10 min and 300 °C for 30 min, respectively. The temperature dependencies of dielectric permittivity and loss were measured at different frequencies using an LCR meter (Agilent, 4284A, Kobe, Hyogo, Japan) connected to a furnace. The current - electric field (*I-E*) and displacement-electric-field (*D-E*) loop and strain - electric field (*S-E*) loop were measured using a ferroelectric hysteresis measurement tester (NPL, UK). The piezoelectric coefficient, d_{33}, was measured on a quasi-static d_{33} meter (CAS, ZJ-3B). Samples used for d_{33} measurements were poled in silicone oil at 180 °C for 20 min under a DC electric field of 13 kV mm^{-1}. Capacitance and loss tangent as a function of frequency were measured using an impedance analyser (Agilent, 4294A, Hyogo, Japan). Dielectric property of the samples at the THz band were measured using a terahertz time-domain spectroscopy (THz-TDS). The details of the setup and experimental producer are

described in the Supporting Information. An elastic vibrational model of an electric dipole under an alternating electric field was constructed and the vibrational dynamics were simulated by Matlab software to demonstrate the differential of a single electric dipole in domain and domain wall.

3. RESULTS AND DISCUSSION

The fitted X-ray diffraction profile of ground CBNRC ceramic powder is shown in Figure S1, with the crystal and refinement parameters summarised in Table S1. Data are in good agreement with the reference pattern for CBNO (JCPDS #49-0608), with no evidence for secondary phases. The coordinates of CBNO reported by Blake et al.[29] in space group $A2_1am$ were used as an initial model for structural refinement, yielding refined lattice parameters of a = 5.4758(2) Å, b = 5.4394(2) Å, and c = 24.887(9) Å at room temperature. The resulting unit cell volume is slightly smaller than that of pure CBNO,[29] despite the fact that the Rb^+ cation has a larger ionic radius than Ca^{2+}, while Ce^{3+} has the same ionic radius as Ca^{2+}.[30] This contraction in unit cell volume might be associated with some volatilization of rubidium during synthesis, but evidence from elemental maps confirms that Rb is present in the sample and is homogenously distributed (Figure S2). The crystal structure of CBNRC is shown in Figure 1, with the polarization direction indicated. A similar level of ferroelectric distortion,[31,32] defined as $100(a/b\text{-}1)$ is seen in CBNRC (0.66%) compared to CBNO (0.75%).

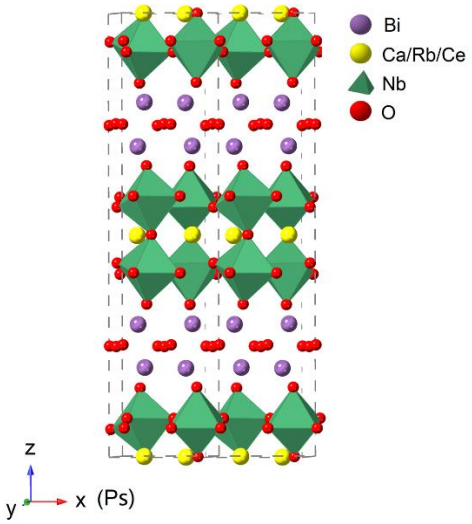

Figure 1. Crystal structure of CBNRC with the polarization direction indicated.

Figure 2a shows the temperature dependence of dielectric permittivity and loss for a CBNRC ceramic. The Curie point (T_c) of CBNRC is 934 °C (±2 °C), slightly lower than the value of 940 °C in pure CBNO, which is consistent to decreased ferroelectric distortion[31] induced by doping. The loss peaks, a few degrees below of T_c, can be attributed to domain wall movement.[26] The frequency-dependence of the dielectric permittivity peaks in the temperature range 600~800 °C typically indicates the presence of oxygen vacancies,[26,33] which commonly occur during high temperature sintering. In Figure 2a, above *T*c, the dielectric permittivity at 10 kHz increased with increasing temperature, but the permittivity decreased at higher frequencies (≥50 kHz). Above *T*c, the decrease of dielectric permittivity in paraelectric phase at high frequency (≥50 kHz) is due to the disappearance of spontaneous polarization. However, besides the spontaneous polarization and related ferroelectric domains, there are additional dipoles which are active at low frequencies and dominate the contribution to dielectric permittivity at low

frequencies. The contributions of these additional dipoles are thermally active and result in the increase of the dielectric permittivity at 10 kHz above *T*c. Current-electric field (*I*-*E*) and displacement-electric-field (*D*-*E*) measurements were carried out, yielding an unsaturated *D*-*E* hysteresis loop and invisible current peaks related to domain switching in the *I*-*E* loop, (not shown). These are due to the evidently high coercive field of CBNRC. CBNRC exhibited a piezoelectric coefficient (d_{33}) value of 7.8 pC N^{-1}, after poling under a DC field of 13 kV mm^{-1} in silicone oil for 20 min at 180 °C, confirming ferroelectric domain switching.

As CBNRC has orthorhombic symmetry, spontaneous polarization is developed along the [100] direction. Both 90° and 180° domain walls, which can be referred to as non-180° and 180° domain walls, are permissible in grains of the ceramic. The motion of 180° domain walls will affect only the dielectric properties while the motion of non-180° domain walls will affect both dielectric and piezoelectric properties.[21,34] Further confirmation of non-180° domain wall switching is seen in the butterfly shape of the strain-electric field (*S*-*E*) loop (Figure 2b). The switching of non-180° domains upon application of the electric field is the major mechanism contributing to the butterfly shaped *S*-*E* loop.[35]

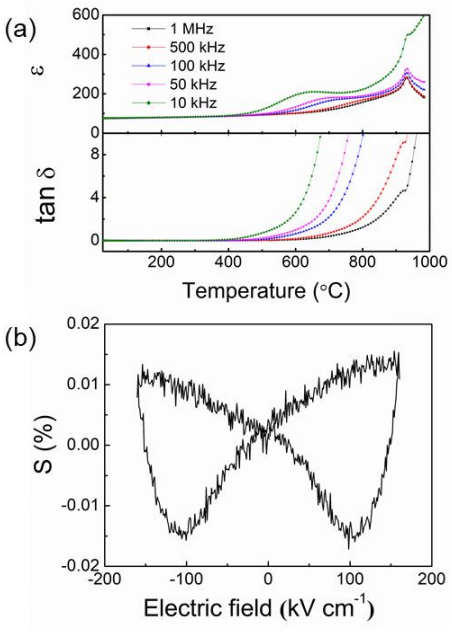

Figure 2. Dielectric and piezoelectric properties of CBNRC ceramics. (a) Temperature dependence of relative dielectric permittivity (ε) and dielectric loss (tan δ); (b) Strain-Electric field (*S*-*E*) loop.

In order to understand the contribution of domain walls to dielectric properties, dielectric permittivity and loss were characterized using impedance spectroscopy and THz-TDS, the results of which are shown in Figure 3. Figure3a shows the dielectric permittivity and loss of a CBNRC ceramic in unpoled and poled states in the frequency range 1 kHz to 1 MHz. The poling process induced irreversible domain wall switching and caused a decrease in domain wall density in the poled sample. Compared with the unpoled sample, the dielectric permittivity of the poled sample decreased, which indicates that the switching of the non-180° domain walls decreases the domain wall density and hence lowers the dielectric response at low frequency after poling.[36] The peaks in ε_r and tan δ plots of the poled ceramic are attributed to the piezoelectric effect. Figure 3b shows the

relative dielectric permittivity and dielectric loss of poled and unpoled CBNRC ceramic at THz frequencies. Relative permittivity is lower at these high frequencies than that at lower frequencies, which is consistent with the fact that there are different dipoles in dielectrics and the dipoles with long relaxation time cannot follow the AC field at higher frequencies.[37–39] Moreover, the dielectric loss at THz frequencies is higher than that at low frequencies, which can be attributed to the dielectric relaxation mechanism happening close to the measured THz band. There are many different polarizations in CBNRC, and some polarizations are active and their relaxation frequencies are close to the measured THz frequencies, which causes dielectric relaxation and related high loss at the THz frequencies. As these relaxation scenarios happen only at the higher frequencies, low frequency measurement won't be able to reflect these high frequency relaxation mechanisms. As shown in Figure 3b, the poled CBNRC sample surprisingly exhibits higher dielectric permittivity and lower dielectric loss than the unpoled sample in the THz frequency range. This appears to contradict the traditional view that the domain wall contribution dies above 10^{10} Hz.[24,37,40] It is worth noting that the unpoled sample shows Fabry-Perot (FP) oscillations,[41] but the poled sample does not. The high permittivity of the poled sample causes significant time delay in the wave propagation inside the sample. This time delay is longer than the detector repetition rate of the THz system and therefore, FP effects are undetectable. For the unpoled sample, equal intervals of ~48 GHz in the lower THz band are observed and matched to the sample thickness (440 μm) and the permittivity (~50). The decreased permittivity at higher THz frequencies (> 0.48 THz) causes a shorter time delay in wave propagation inside the sample, resulting in an increase in the interval frequency of FP oscillations. The FP oscillations show relatively

shifted frequencies in permittivity and loss tangent, caused by the higher loss tangent values of the unpoled sample.[41]

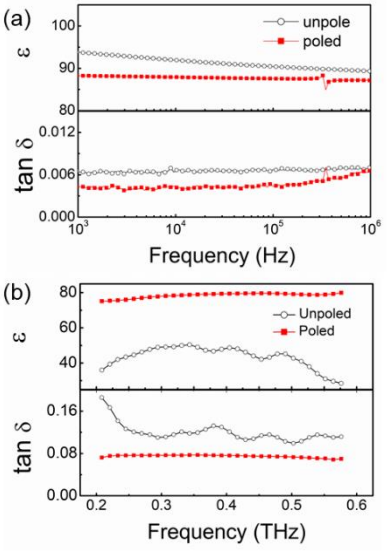

Figure 3. Dielectric properties of CBNRC ceramic at different frequencies. (a) Dielectric properties at kHz frequencies; (b) Dielectric properties at THz frequencies.

To explain the differences in dielectric behaviour of CBNRC ceramic in different states (poled and unpoled) and in different frequency ranges, the domain wall contribution was analysed from the macroscopic and microscopic perspectives. As described above, the dielectric permittivity mainly consists of contributions from lattice level intrinsic polarization, defects and domain wall motion. Thus, the dielectric permittivity can be denoted as:

$$\varepsilon = \varepsilon_{in} + \varepsilon_{def} + \varepsilon_{DW-non180} + \varepsilon_{DW-180}$$

where ε_{in} is the intrinsic contribution to permittivity, ε_{def} is a point defect contribution (mainly from oxygen vacancies, V_O''), $\varepsilon_{DW-non180}$ is the non-180° domain wall contribution and ε_{DW-180} is the 180° domain wall contribution. While the relaxation

frequency of intrinsic polarization lies beyond THz frequencies,[39,42] the point defects in CBNRC are mainly active at low frequencies, which is supported by the fact that the V_O'' related dielectric peaks are greatly weakened with increasing frequency in Figure 2a. The domain walls, however, will contribute to dielectric permittivity differently at different frequencies. Figure 4a and b show illustrations of non-180° and 180° ferroelectric domains with detail of the corresponding domain walls shown in Figure 4c and d. In order to minimize the free energy with the gradient change of polarization across the domain wall, weak dipoles (frustrated dipoles) develop within the domain walls (Figure 4c and Figure 4d).[18,43–45] Figure 4e shows a schematic representation of the variation of Gibbs free energy, *G*, with electric displacement for domains and domain walls, the polar vectors of which are in the [-100] and [100] directions. At temperatures lower than T_c, there are two minima for domains and domain walls on the free-energy profile[46] and thus, the ferroelectric phase is stable. From thermodynamic theory, the dielectric displacement is the first derivative of *G* with respect to electric field ($D = \frac{\partial G}{\partial E}$). As the domain walls are made up of frustrated dipoles within nano scaled interfaces, the dielectric displacement of domain walls, D_{S2} is smaller than that of domains, D_{S1}.[16] At low frequencies, all the dipoles within the domain walls are able to follow the AC field and each domain wall is active as a group. The non-180° domain walls will increase dielectric permittivity[47] and the 180° domain walls will decrease permittivity because of their clamping effect.[48–50] The decreased dielectric permittivity in poled samples at low frequencies (Figure 4a) indicates that the positive contribution from $\varepsilon_{DW-non180}$ is the dominant factor between the competitive effects of $\varepsilon_{DW-non180}$ and ε_{DW-180}. At THz frequencies, the local lattices within domain walls are active as single frustrated dipoles instead of a group. The

permittivity of a single frustrated dipole in domain wall is smaller than its counterpart in domain. The contribution of a single dipole in the lattice (either in a domain or a domain wall) to dielectric permittivity can be calculated using an elastic vibration model (see Figure 4f and the Supporting information).[42] The contribution to permittivity from a dipole in a domain is higher than that from one in a domain wall. This is in good agreement with our experimental results that the dielectric permittivity is higher in the poled ceramic at THz frequencies, due to its lower domain wall density.

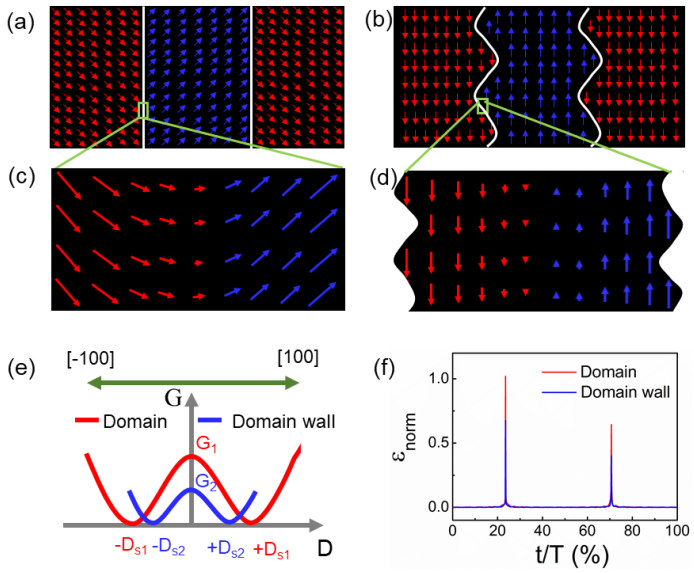

Figure 4. Illustration of ferroelectric domains and domain walls and their dynamics. (a) Non-180° domains; (b) 180° domains; (c) Non-180° domain walls; (d) 180° domain-walls; (e) Variation of free energy of domain and domain walls with displacement; (f) Simulated permittivity contribution of a single dipole in a domain (red) or domain wall (blue), where ε_{norm} is the normalised permittivity $\varepsilon/\varepsilon_{max(domain)}$, *x*-axis is the percentage of cycle period.

As the domain wall dynamics of ferroelectrics are active in the THz band, they can be utilized in new and viable applications, such as low loss dielectrics and non-destructive read-out ferroelectric memory driven by THz technologies through domain wall engineering. For new dielectrics to be used at THz frequencies, materials should have moderate dielectric permittivity and low dielectric loss.[51] Figure S6 displays the dielectric properties of different ferroelectric materials summarized from the literature at 0.5 THz. The CBNRC ceramic produced in this work has medium dielectric permittivity and low dielectric loss in the THz band. The dielectric permittivity of CBNRC doubles on poling and the dielectric loss decreases, indicating its suitability for dielectric applications at these frequencies. A proposed application for this effect is non-destructive read-out dielectric memory. Previously, read-out of ferroelectric memory has been mainly based on destructive bipolar [52] or domain-wall-type resistance[53] switching. The disadvantage of the former technique is its destructive nature, while the latter is limited the low current generated from these switches which is insufficient to drive read-out circuits. Figure 5 shows the proposed mechanism of THz reading of dielectric switching memory, where dielectric permittivity can be modulated by domain wall dielectric switching through poling and depoling. The morphology of 90° and 180° domain walls is demonstrated using straight lines and curves.[54] Here, poling or depoling are used to facilitate the writing process; the poled state is achieved by an applied DC field and the depoled state is achieved by a reverse bias DC field, because a poled ferroelectric can be depolarized when the reversal field is applied at the negative coercive field, which enables to achieve a reversed and erasable memory. The domain wall density is low in the poled state and high in the depoled state, reflective of high and low dielectric permittivity at THz

frequencies, respectively. For dielectric memory applications, the modulated permittivity is compared with a set 'gate' permittivity and then marked as state 'off' if it is below or 'on' if it is above this value. These 'off' and 'on' states correspond to '0' and '1' digital positions, which can be spontaneously read by THz probe signaling. This non-destructive read mechanism could pave the way for the development of next generation THz ferroelectric devices.

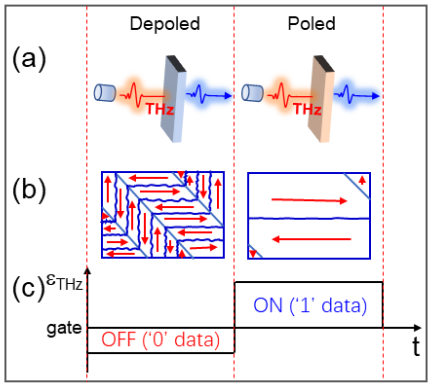

Figure 5. Illustration of non-destructive read-out dielectric switching memory. (a) Schematic setup of THz reading technology; (b) Domain wall density change in depoled and poled ferroelectric; (c) THz reading of off/on (0/1) positions. Dashed lines denote depoled and poled states.

4. CONLUSIONS

In summary, the dynamics of domain walls in the CBNRC ferroelectric ceramic have been read using THz Time domain spectroscopy, and which are compared with the contribution from the low frequency impedance spectroscopy. The results show that non-180° domain walls actively contribute to high permittivity at the low frequencies. At the THz band, domain walls are non-active as a group due to their long relaxation time, and they work as defective interface originated from their frustrated dipoles. These unfulfilled

dipoles in the domain walls contribute less to the permittivity compared with their counterparts in domains. The experimental results are theoretically supported by an elastic vibration model. The work here shows that field induced changes in domain wall density are detectable at high frequencies and are related to lattice level dynamics of dipoles in ferroelectrics. This observation could lead to new THz frequency applications for ferroelectrics such as domain wall dielectric switching memory.

ASSOCIATED CONTENT

Supporting Information.

Experimental procedures, full spectrum of XRD results and refined data, simulation of permittivity for single dipole in domain and domain wall, comparison of dielectric properties between the current material in this paper with other ferroelectrics, are included in the supporting information.

AUTHOR INFORMATION

Corresponding Author

*B. Yang: b.yang@chester.ac.uk;

*D. Zhang: dzhang@csu.edu.cn;

*H. Yan: h.x.yan@qmul.ac.uk

Author Contributions

The manuscript was written through contributions of all authors. All authors have given approval to the final version of the manuscript.

Funding Sources

H. Yan thanks the financial support from the Engineering and Physical Sciences Research Council (EPSRC) (MASSIVE Project, EP/L017695/1) and the Royal Society for a Newton Advanced Fellowship award (NAF\R1\201126). M. Zhang thanks the financial support from China Scholarship Council (CSC, 201706370172). D. Zhang thanks the National Natural Science Foundation of China (Grant No. U19A2087) for the financial support. D. Zhang and H. Yan thank the financial support from Guangzhou Guangding Technology Group Co. Ltd.

Notes

The authors declare no competing financial interests in this work.

REFERENCES

(1) Prateek; Thakur, V. K.; Gupta, R. K. Recent Progress on Ferroelectric Polymer-Based Nanocomposites for High Energy Density Capacitors: Synthesis, Dielectric Properties, and Future Aspects. *Chemical Reviews*. **2016**, *116*, 4260-4317.

(2) Muralt, P. Ferroelectric Thin Films for Micro-Sensors and Actuators: A Review. *J. Micromechanics Microengineering* **2000**, *10*, 136.

(3) Zhang, S.; Yu, F. Piezoelectric Materials for High Temperature Sensors. *J. Am. Ceram. Soc.* **2011**, *94*, 3153-3170.

(4) De Araujo, C. A. P.; Cuchiaro, J. D.; Mc Millan, D. L.; Scott, M. C.; Scott, J. F. Fatigue-Free Ferroelectric Capacitors with Platinum Electrodes. *Nature* **1995**, *374*, 627-629.

(5) Park, B. H.; Kang, B. S.; Bu, S. D.; Noh, T. W.; Lee, J.; Jo, W. Lanthanum-

Substituted Bismuth Titanate for Use in Non-Volatile Memories. *Nature* **1999**, *401* (6754), 682–684.

(6) Ma, C.; Luo, Z.; Huang, W.; Zhao, L.; Chen, Q.; Lin, Y.; Liu, X.; Chen, Z.; Liu, C.; Sun, H.; Jin, X.; Yin, Y.; Li, X. Sub-Nanosecond Memristor Based on Ferroelectric Tunnel Junction. *Nat. Commun.* **2020**, *11*, 1-9.

(7) Li, J. Y.; Rogan, R. C.; Üstündag, E.; Bhattacharya, K. Domain Switching in Polycrystalline Ferroelectric Ceramics. *Nat. Mater.* **2005**, *4*, 776-781.

(8) Jesse, S.; Rodriguez, B. J.; Choudhury, S.; Baddorf, A. P.; Vrejoiu, I.; Hesse, D.; Alexe, M.; Eliseev, E. A.; Morozovska, A. N.; Zhang, J.; Chen, L. Q.; Kalinin, S. V. Direct Imaging of the Spatial and Energy Distribution of Nucleation Centres in Ferroelectric Materials. *Nat. Mater.* **2008**, *7*, 209-215.

(9) Ma, H.; Gao, W.; Wang, J.; Wu, T.; Yuan, G.; Liu, J.; Liu, Z. Ferroelectric Polarization Switching Dynamics and Domain Growth of Triglycine Sulfate and Imidazolium Perchlorate. *Adv. Electron. Mater.* **2016**, *2*, 1600038.

(10) Li, Y.; Sun, N.; Li, X.; Du, J.; Chen, L.; Gao, H.; Hao, X.; Cao, M. Multiple Electrical Response and Enhanced Energy Storage Induced by Unusual Coexistent-Phase Structure in Relaxor Ferroelectric Ceramics. *Acta Mater.* **2018**, *146*, 202-210.

(11) Li, Y.; Sun, N.; Du, J.; Li, X.; Hao, X. Stable Energy Density of a PMN-PST Ceramic from Room Temperature to Its Curie Point Based on the Synergistic Effect of Diversified Energy. *J. Mater. Chem. C* **2019**, *7*, 7692-7699.

(12) Pan, H.; Li, F.; Liu, Y.; Zhang, Q.; Wang, M.; Lan, S.; Zheng, Y.; Ma, J.; Gu, L.; Shen, Y.; Yu, P.; Zhang, S.; Chen, L. Q.; Lin, Y. H.; Nan, C. W. Ultrahigh–Energy

Density Lead-Free Dielectric Films via Polymorphic Nanodomain Design. *Science.* **2019**, *365*, 578-582.

(13) Qi, H.; Zuo, R.; Xie, A.; Tian, A.; Fu, J.; Zhang, Y.; Zhang, S. Ultrahigh Energy-Storage Density in $NaNbO_3$-Based Lead-Free Relaxor Antiferroelectric Ceramics with Nanoscale Domains. *Adv. Funct. Mater.* **2019**, *29*, 1903877.

(14) Luo, N.; Han, K.; Cabral, M. J.; Liao, X.; Zhang, S.; Liao, C.; Zhang, G.; Chen, X.; Feng, Q.; Li, J. F.; Wei, Y. Constructing Phase Boundary in $AgNbO_3$ Antiferroelectrics: Pathway Simultaneously Achieving High Energy Density and Efficiency. *Nat. Commun.* **2020**, *11*, 1-10.

(15) Gu, Z.; Pandya, S.; Samanta, A.; Liu, S.; Xiao, G.; Meyers, C. J. G.; Damodaran, A. R.; Barak, H.; Dasgupta, A.; Saremi, S.; Polemi, A.; Wu, L.; Podpirka, A. A.; Will-Cole, A.; Hawley, C. J.; Davies, P. K.; York, R. A.; Grinberg, I.; Martin, L. W.; Spanier, J. E. Resonant Domain-Wall-Enhanced Tunable Microwave Ferroelectrics. *Nature* **2018**, *560*, 622-627.

(16) Li, F.; Lin, D.; Chen, Z.; Cheng, Z.; Wang, J.; Li, C.; Xu, Z.; Huang, Q.; Liao, X.; Chen, L. Q.; Shrout, T. R.; Zhang, S. Ultrahigh Piezoelectricity in Ferroelectric Ceramics by Design. *Nat. Mater.* **2018**, *17*, 349–354.

(17) Li, P.; Zhai, J.; Shen, B.; Zhang, S.; Li, X.; Zhu, F.; Zhang, X. Ultrahigh Piezoelectric Properties in Textured $(K,Na)NbO_3$-Based Lead-Free Ceramics. *Adv. Mater.* **2018**, *30*, 1–9.

(18) Liu, S.; Cohen, R. E. Origin of Stationary Domain Wall Enhanced Ferroelectric Susceptibility. *Phys. Rev. B* **2017**, *95*, 1–9.

(19) Spaldin, N. A. Fundamental Size Limits in Ferroelectricity. *Science*. **2004**, *304*,

1606-1607.

(20) Kingon, A. I.; Srinivasan, S. Lead Zirconate Titanate Thin Films Directly on Copper Electrodes for Ferroelectric, Dielectric and Piezoelectric Applications. *Nat. Mater.* **2005**, *4*, 233-237.

(21) Zhang, Q. M.; Wang, H.; Kim, N.; Cross, L. E. Direct Evaluation of Domain-Wall and Intrinsic Contributions to the Dielectric and Piezoelectric Response and Their Temperature Dependence on Lead Zirconate-Titanate Ceramics. *J. Appl. Phys.* **1994**, *75*, 454–459.

(22) Xu, F.; Trolier-McKinstry, S.; Ren, W.; Xu, B.; Xie, Z. L.; Hemker, K. J. Domain Wall Motion and Its Contribution to the Dielectric and Piezoelectric Properties of Lead Zirconate Titanate Films. *J. Appl. Phys.* **2001**, *89*, 1336–1348.

(23) Morozovska, A. N.; Eliseev, E. A.; Varenyk, O. V.; Kalinin, S. V. Effective Piezoelectric Response of Twin Walls in Ferroelectrics. *J. Appl. Phys.* **2013**, *113*, 187222.

(24) Tsurumi, T.; Li, J.; Hoshina, T.; Kakemoto, H.; Nakada, M.; Akedo, J. Ultrawide Range Dielectric Spectroscopy of $BaTiO_3$-Based Perovskite Dielectrics. *Appl. Phys. Lett.* **2007**, *91*, 10–13.

(25) Yan, H.; Zhang, H.; Ubic, R.; Reece, M. J.; Liu, J.; Shen, Z.; Zhang, Z. A Lead-Free High-Curie-Point Ferroelectric Ceramic, $CaBi_2Nb_2O_9$. *Adv. Mater.* **2005**, *17*, 1261–1265.

(26) Yan, H.; Zhang, H.; Reece, M. J.; Dong, X. Thermal Depoling of High Curie Point Aurivillius Phase Ferroelectric Ceramics. *Appl. Phys. Lett.* **2005**, *87*, 1–4.

(27) Newnham, R. E.; Wolfe, R. W.; Dorrian, J. F. Structural Basis of Ferroelectricity

in the Bismuth Titanate Family. *Mater. Res. Bull.* **1971**, *6*, 1029–1039.

(28) Zhang, H.; Yan, H.; Reece, M. J. Microstructure and Electrical Properties of Aurivillius Phase $(CaBi_2Nb_2O_9)_{1-x}(BaBi_2Nb_2O_9)_x$ Solid Solution. *J. Appl. Phys.* **2010**, *108*, 014109.

(29) Blake, S. M.; Falconer, M. J.; McCreedy, M.; Lightfoot, P. Cation Disorder in Ferroelectric Aurivillius Phases of the Type $Bi_2ANb_2O_9$ (A = Ba, Sr, Ca). *J. Mater. Chem.* **1997**, *7*, 1609–1613.

(30) Shannon, R. D. Revised Effective Ionic Radii and Systematic Studies of Interatomic Distances in Halides and Chalcogenides. *Acta Crystallogr. Sect. A* **1976**, *32*, 751–767.

(31) Viola, G.; Boon Chong, K.; Eriksson, M.; Shen, Z.; Zeng, J.; Yin, Q.; Kan, Y.; Wang, P.; Ning, H.; Zhang, H.; Fitzpatrick, M. E.; Reece, M. J.; Yan, H. Effect of Grain Size on Domain Structures, Dielectric and Thermal Depoling of Nd-Substituted Bismuth Titanate Ceramics. *Appl. Phys. Lett.* **2013**, *103*, 182903.

(32) Zhao, Z.; Buscaglia, V.; Viviani, M.; Buscaglia, M. T.; Mitoseriu, L.; Testino, A.; Nygren, M.; Johnsson, M.; Nanni, P. Grain-Size Effects on the Ferroelectric Behavior of Dense Nanocrystalline $BaTiO_3$ Ceramics. *Phys. Rev. B - Condens. Matter Mater. Phys.* **2004**, *70*, 1–8.

(33) Tan, Y.; Zhang, J.; Wu, Y.; Wang, C.; Koval, V.; Shi, B.; Ye, H.; McKinnon, R.; Viola, G.; Yan, H. Unfolding Grain Size Effects in Barium Titanate Ferroelectric Ceramics. *Sci. Rep.* **2015**, *5*, 15–21.

(34) Zheng, T.; Wu, J.; Cheng, X.; Wang, X.; Zhang, B.; Xiao, D.; Zhu, J.; Wang, X.; Lou, X. High Strain in $(K_{0.40}Na_{0.60})(Nb_{0.955}Sb_{0.045})O_3$-$Bi_{0.50}Na_{0.50}ZrO_3$ Lead-Free

Ceramics with Large Piezoelectricity. *J. Mater. Chem. C* **2014**, *2*, 8796–8803.

(35) Viola, G.; Saunders, T.; Wei, X.; Chong, K. B.; Luo, H.; Reece, M. J.; Yan, H. Contribution of Piezoelectric Effect, Electrostriction and Ferroelectric/Ferroelastic Switching to Strain-Electric Field Response of Dielectrics. *J. Adv. Dielectr.* **2013**, *03*, 1350007.

(36) Tan, Y.; Viola, G.; Koval, V.; Yu, C.; Mahajan, A.; Zhang, J.; Zhang, H.; Zhou, X.; Tarakina, N. V.; Yan, H. On the Origin of Grain Size Effects in $Ba(Ti_{0.96}Sn_{0.04})O_3$ Perovskite Ceramics. *J. Eur. Ceram. Soc.* **2019**, *39*, 2064–2075.

(37) Hoshina, T.; Kigoshi, Y.; Hatta, S.; Teranishi, T.; Takeda, H.; Tsurumi, T. Size Effect and Domain-Wall Contribution of Barium Titanate Ceramics. *Ferroelectrics* **2010**, *402*, 29–36.

(38) Zhu, L.; Wang, Q. Novel Ferroelectric Polymers for High Energy Density and Low Loss Dielectrics. *Macromolecules* **2012**, *45*, 2937–2954.

(39) Wu, J.; Sun, W.; Meng, N.; Zhang, H.; Koval, V.; Zhang, Y.; Donnan, R.; Yang, B.; Zhang, D.; Yan, H. Terahertz Probing Irreversible Phase Transitions Related to Polar Clusters in $Bi_{0.5}Na_{0.5}TiO_3$-Based Ferroelectric. *Adv. Electron. Mater.* **2020**, *6*, 1901373.

(40) Tsykalov, V. G.; Poplavko, Y. M. Permittivity Dispersion of Various Ferro-and Antiferroelectrics in the Millimetre Wave-Length Range above the Curie Point. *Izv. Akad. Nauk SSSR* **1970**, *34*, 2586–2589.

(41) Yang, B.; Wylde, R. J.; Martin, D. H.; Goy, P.; Donnan, R. S.; Caroopen, S. Determination of the Gyrotropic Characteristics of Hexaferrite Ceramics from 75 to 600 GHz. *IEEE Trans. Microw. Theory Tech.* **2010**, *58* , 3587–3597.

(42) Barsoum, M. Fundamentals of Ceramics. CRC press, 2019.

(43) Lee, D.; Behera, R. K.; Wu, P.; Xu, H.; Sinnott, S. B.; Phillpot, S. R.; Chen, L. Q.; Gopalan, V. Mixed Bloch-Néel-Ising Character of 180° ferroelectric Domain Walls. *Phys. Rev. B - Condens. Matter Mater. Phys.* **2009**, *80*, 2–5.

(44) Jia, C. L.; Mi, S. B.; Urban, K.; Vrejoiu, I.; Alexe, M.; Hesse, D. Atomic-Scale Study of Electric Dipoles near Charged and Uncharged Domain Walls in Ferroelectric Films. *Nat. Mater.* **2008**, *7*, 57–61.

(45) Nelson, C. T.; Winchester, B.; Zhang, Y.; Kim, S. J.; Melville, A.; Adamo, C.; Folkman, C. M.; Baek, S. H.; Eom, C. B.; Schlom, D. G.; Chen, L. Q.; Pan, X. Spontaneous Vortex Nanodomain Arrays at Ferroelectric Heterointerfaces. *Nano Lett.* **2011**, *11*, 828–834.

(46) Lines, M. E.; Glass, A. M. Principles and Applications of Ferroelectrics and Related Materials. Oxford university press, 2001.

(47) Xu, R.; Karthik, J.; Damodaran, A. R.; Martin, L. W. Stationary Domain Wall Contribution to Enhanced Ferroelectric Susceptibility. *Nat. Commun.* **2014**, *5*, 1–7.

(48) Drougard, M. E.; Young, D. R. Domain Clamping Effect in Barium Titanate Single Crystals. *Phys. Rev.* **1954**, *94*, 1561.

(49) Zhang, H.; Yang, B.; Yan, H.; Abrahams, I. Isolation of a Ferroelectric Intermediate Phase in Antiferroelectric Dense Sodium Niobate Ceramics. *Acta Mater.* **2019**, *179*, 255–261.

(50) Yan, Z.; Zhang, D.; Zhou, X.; Zhang, M.; Yue, Y.; Zhang, L.; Xue, G.; Luo, H.; Abrahams, I.; Yan, H. Phase Transitions in $RbPrNb_2O_7$, a Layer Structured Ferroelectric with a High Curie Point. *Acta Mater.* **2020**, *200*, 971–979.

(51) Kong, L. B.; Li, S.; Zhang, T. S.; Zhai, J. W.; Boey, F. Y. C.; Ma, J. Electrically Tunable Dielectric Materials and Strategies to Improve Their Performances. *Prog. Mater. Sci.* **2010**, *55*, 840–893.

(52) Blom, P. W. M.; Wolf, R. M.; Cillessen, J. F. M.; Krijn, M. P. C. M. Ferroelectric Schottky Diode. *Phys. Rev. Lett.* **1994**, *73*, 2107–2110.

(53) Jiang, J.; Bai, Z. L.; Chen, Z. H.; He, L.; Zhang, D. W.; Zhang, Q. H.; Shi, J. A.; Park, M. H.; Scott, J. F.; Hwang, C. S.; Jiang, A. Q. Temporary Formation of Highly Conducting Domain Walls for Non-Destructive Read-out of Ferroelectric Domain-Wall Resistance Switching Memories. *Nat. Mater.* **2018**, *17*, 49–55.

(54) Cheng, S. Y.; Ho, N. J.; Lu, H. Y. Transformation-Induced Twinning: The 90° and 180° Ferroelectric Domains in Tetragonal Barium Titanate. J. Am. Ceram. Soc. **2006**, *89*, 2177–2187.

Graphic for manuscript